Difluoroboron Chelation to Quinacridonequinone: A New Synthetic Method for Air-Sensitive 6,13-Dihydroxyquinacridone *via* Boron Complexes

Koichiro Moriya, Ryohei Shimada, and Katsuhiko Ono*[a]

Abstract: This study aims to perform the chelation of difluoroboron (BF_2) to quinacridonequinone (QQ). The resulting dark green solid was determined to be QA-BF_2, which is a BF_2 complex of 6,13-dihydroxyquinacridone (QA-OH), and not QQ-BF_2, which is a BF_2 complex of QQ. This result indicated that QQ-BF_2 was first generated as an *O,O*-bidentate chelate, which immediately underwent a two-electron reduction to produce QA-BF_2. This compound was converted to air-sensitive QA-OH by undergoing hydrolysis in argon. Since QA-OH has a strong electron-donating property, it easily produced QQ *via* air oxidation in the solution. QA-OH also acts as a reducing reagent for quinones. The crystal packing of QA-OH is a herringbone type with short π···π contacts, and a good hole mobility has been suggested by the theoretical calculations. Herein, a new synthetic method from QQ to QA-OH using BF_2 chelation and hydrolysis was proposed. QA-BF_2 and QA-OH are useful organic functional pigments and reducing reagents.

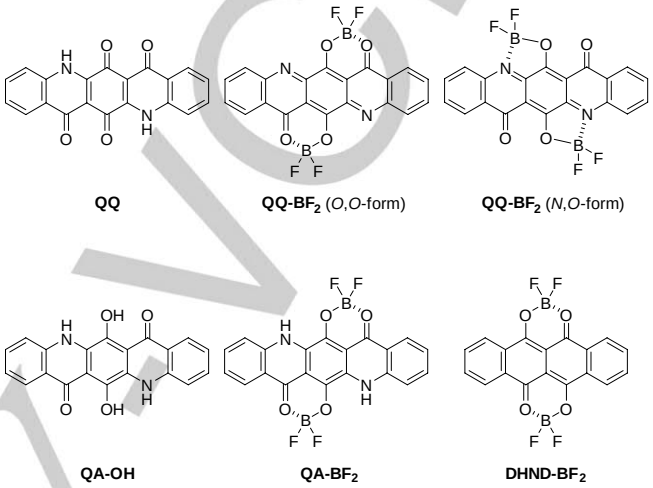

Scheme 1. Structure of BF_2 complexes and quinacridone derivatives.

Organoboron complexes of *β*-diketonate, *β*-ketoiminate, and *β*-diiminate and their analogs have attracted a significant amount of attention owing to their unique fluorescence, phosphorescence, and redox properties and polar structures.[1–6] Their fields of application are diverse as well as boron-dipyrromethane (BODIPY). They have been applied to mechanofluorochromism,[7] bioimaging,[8] molecular assembly,[9] organic light-emitting diodes (OLEDs),[10] solar cells,[11] memory devices,[12] organic field-effect transistors (OFETs),[13] and sensing for oxygen,[14] ions,[15] and other external stimuli.[16] The functionalization with organoboron chelation primarily involves modifying or enhancing the ligand performance. Furthermore, recent studies have utilized the BF_2 complex as a reaction catalyst or substance.[17] These complexes are useful for the synthetic reactions of new compounds.

On the contrary, quinacridone (QA) derivatives are synthetic pigments that have a vivid color and weather resistance and are used in various industrial applications.[18] They exhibit red to purple color in the solid state but exhibit yellowish color in solution. This change in color in the solid state arises from intermolecular interactions *via* hydrogen bonds. They have also been investigated as emitters in OLEDs[19] and as p-type semiconductors in OFETs[20] or organic photovoltaics (OPVs).[21] Since QA is one of the important components in industrial organic pigments, the difluoroboron (BF_2) chelation of quinacridonequinone (QQ), which is a member of the QA group compounds, is of interest for the development of new pigments. Prior to this study, we previously reported the structures and properties of DHND-BF_2 and F-DHND-BF_2, which are BF_2 complexes of 6,11-dihydroxy-5,12-naphthacenedione (DHND) and its perfluoro derivative (F-DHND).[5a,b] These compounds exhibit n-type semiconductor performance in OFETs owing to their high electron affinities.

The BF_2 chelation of QQ produced a dark green solid. This was predicted to be either of the two geometric isomers of QQ-BF_2 (the *O,O*- or *N,O*-bidentate chelate form); however, it was a BF_2 complex of 6,13-dihydroxyquinacridone (QA-OH) and was determined as QA-BF_2 (Scheme 1). Furthermore, when the boron chelate of QA-BF_2 was removed *via* hydrolysis in argon, air-sensitive QA-OH was obtained as a dark purple solid.[22] To the best of our knowledge, this conversion from QQ to QA-OH is the first example of a synthetic method based on the electron affinity of the BF_2 complex, and it is useful for the development of new functional dyes and pigments. Herein, we report the structures, reactions, and properties of QA-BF_2 and QA-OH.

The BF_2 chelation was performed by heating a mixture of QQ and boron trifluoride diethyl etherate ($BF_3{\cdot}OEt_2$) at reflux to produce a dark green solid (Supporting Information). This compound is stable in air in the solid state (M.p. > 300 °C) but unstable in solution because it undergoes hydrolysis. However, it was possible to obtain the ^{1}H NMR spectrum of the product by promptly measuring it in [D_6]DMSO (Figure S1 in the Supporting Information). In a magnetic field ranging from 7 to 9 ppm, four signals that were assigned to aromatic protons were observed. A broad signal was also found at 14.1 ppm. Since the ^{1}H NMR spectrum showed a decrease in the signal after adding a drop of

[a] K. Moriya, R. Shimada, Prof. Dr. K. Ono
Graduate School of Engineering
Nagoya Institute of Technology
Gokiso, Showa-ku, Nagoya 466-8555 (Japan)
E-mail: ono.katsuhiko@nitech.ac.jp

Supporting information and the ORCID identification number(s) for the author(s) of this article can be found under:https://doi.org/10.1002/

D_2O to the solution, the broad signal was assigned to an NH or OH proton. This result indicated that the product was neither the *O*,*O*-form nor the *N*,*O*-form of QQ-BF_2. Additionally, a yellow solid of QQ gradually precipitated upon standing the solution in air.

X-ray crystallography was performed to determine the molecular structure of the dark green solid.[23] A single crystal was obtained by slowly cooling the hot anhydrous DMF solution of the solid. The molecular structure was determined to be QA-BF_2 (Figure 1A). The bond lengths in the central six-membered ring were compared with those of QA and anthraquinone (AQ),[24] as shown in Figure 2. The six-membered ring is not a quinone form similar to AQ but an aromatic form similar to QA. Furthermore, the C–O single bond length is 1.356(4) Å, which is longer than 1.217(2) Å for the C–O double bond in AQ. Thus, the product was determined to be QA-BF_2. The molecular structure is centrosymmetric, and the quinacridone moiety is nearly planar. This crystal contains two DMF molecules per QA-BF_2 molecule. The QA-BF_2 molecules stack along the *a* axis (Figure 1B), and short F···C contacts [3.089(5) Å] were observed. This contact distance is shorter than the sum of the van der Waals radii of the fluorine and carbon atoms (3.17 Å). Since the molecular stacking is governed by these short contacts, the π···π overlap region between quinacridone moieties is small (Figure 1C). Moreover, the molecules form a tape-like structure with short F···H-C contacts (Figure 1D). The contact distance between the F and H atoms is 2.401 Å, which is shorter than the sum of their van der Waals radii (2.67 Å). These molecular arrangements are similar to those found in the crystal of F-DHND-BF_2.[5b]

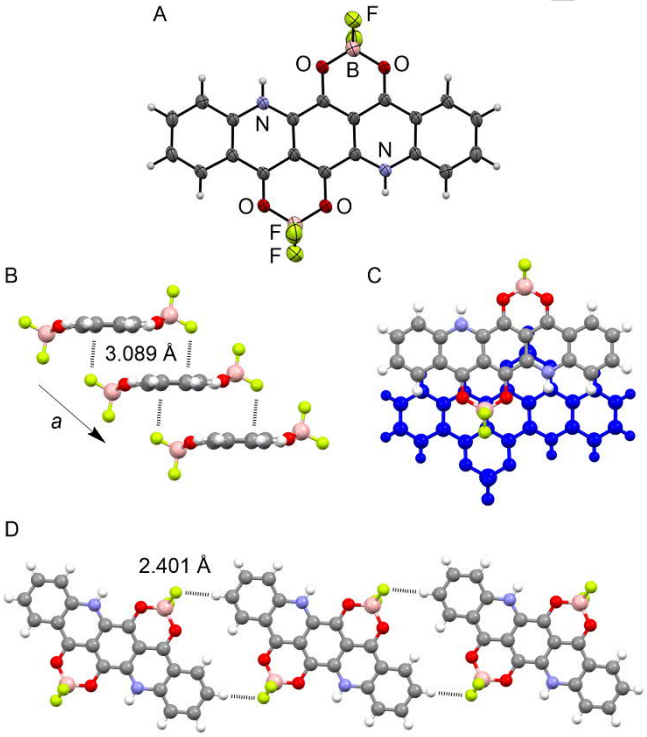

Figure 1. Crystal structure of QA-BF_2: A) molecular structure drawn at the 50% probability level (ORTEP), B) molecular stacking, C) overlap mode, and D) molecular tape.

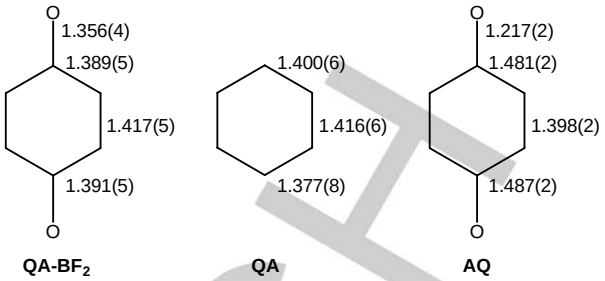

Figure 2. Bond lengths [Å] in the central six-membered rings of QA-BF_2, QA, and AQ as measured *via* X-ray crystallography. These rings are centrosymmetric.

The UV/Vis spectrum of the dark green solid in DMSO showed long-wavelength absorptions with maxima at 688 and 743 nm (sh), and a short-wavelength absorption with a maxima at 318 nm (Figure 3A). The spectra of QA-BF_2 and QQ-BF_2 (*O*,*O*-form) were simulated by time-dependent density functional theory (TDDFT) calculations at the B3LYP/6-31G(d) level,[25] which are shown in Figures 3B and 3C, respectively. The long-wavelength excitation energies (oscillator strengths) of QA-BF_2 and QQ-BF_2 are 681 (0.079) and 527 nm (0.64), respectively. The experimental spectrum agreed well with the simulated spectrum of QA-BF_2. Thus, the dark green solid was conclusively determined to be QA-BF_2. To investigate the electron affinity of QA-BF_2, cyclic voltammetry (CV) experiments were performed in a DMSO solution with 0.1 M $n$$Bu_4NClO_4$. The voltammogram showed two reversible reduction waves and one irreversible oxidation wave (Figure S2 in the Supporting Information). The

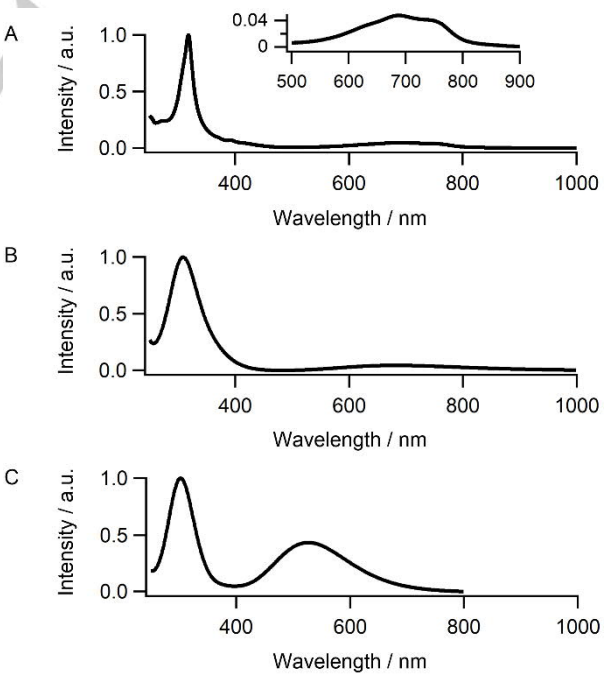

Figure 3. UV/Vis spectra. A) Measurement in DMSO solution. Simulations of B) QA-BF_2 and C) QQ-BF_2 (*O*,*O*-form) calculated using TDDFT at the B3LYP/6-31G(d) level.

half-wave reduction potentials (E_{red}) of QA-BF_2 were observed at −1.00 and −1.44 V versus Fc/Fc^+. Therefore, the electron affinity of QA-BF_2 is slightly higher than that of QQ (E_{red}: −1.15 V) but much lower than that of DHND-BF_2 (E_{red}: −0.33 and −0.81 V). Furthermore, the peak oxidation potential (E_p^{ox}) was observed at +0.38 V, and QA-BF_2 showed a strong electron-donating ability. This suggested that QQ-BF_2 has a high electron affinity.

Based on the above experimental data, we determined that QA-BF_2 was obatined as a dark green solid *via* the reaction of QQ with $BF_3{\cdot}OEt_2$. This indicated that QQ-BF_2 was first generated and immediately underwent a two-electron reduction to form QA-BF_2, although the electron source has not been specified. When the green solution of QA-BF_2 was hydrolyzed in air, a yellow solution of QQ was obtained. Scheme 2 illustrates the outline of these reactions. The hydrolysis of QA-BF_2 in argon provided a dark blue solution of QA-OH, indicating that QQ was generated *via* air oxidation of QA-OH. To investigate the hydrolysis reaction from QA-BF_2 to QA-OH in detail, time-dependent ^1H NMR spectra of QA-BF_2 in [D_6]DMSO containing 4 vol% of H_2O in argon were measured. These spectra and abundance ratio of compounds are shown in Figures S3 and S4 (in the Supporting Information), respectively. After 1 h of the reaction, the monoBF_2 ratio reached 45%, and within 4 h, QA-BF_2 disappeared. After 5 h, the ratio of QA-OH reached 80%, and after 8 h, it ranged between 90% and 96%. The conversion ratio from QA-BF_2 to QA-OH depended upon the amount of water in the DMSO, and the hydrolysis quantitatively proceeded when using 5 vol% or more water at room temperature. QA-OH was stable in solution in argon. However, when the solution was left in air, QQ precipitated. When the hydrolysis of QA-BF_2 was performed in the presence of equimolar benzoquinone, hydroquinone was produced, as shown in Figure 4. The other available quinones are in Figure S5 (Supporting Information).

In the UV/Vis spectrum of QA-OH in DMSO, characteristic absorption bands with a maxima at 577 and 605 nm were observed (Figure S6 in the Supporting Information). According to the TDDFT calculations, the corresponding excitation energy (oscillator strength) was 557 nm (0.087), which supports the molecular structure. The CV experiments of QA-OH in DMSO

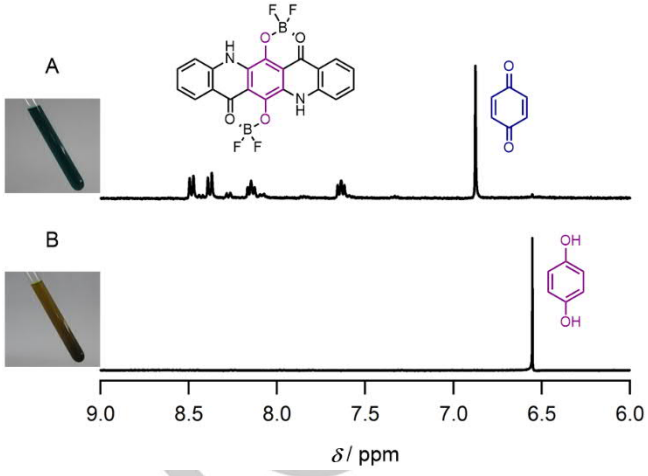

Figure 4. ^1H NMR (400 MHz) spectra of the mixture of QA-BF_2 and benzoquinone (1:1 molar ratio) in [D_6]DMSO containing 4 vol% of water in argon: A) immediately after beginning the reaction and B) after 24 h. These spectra indicate the reduction of benzoquinone to hydroquinone by QA-OH generated in the hydrolysis of QA-BF_2. No peaks attributed to QQ were observed at the end of the reaction because QQ precipitated because of its poor solubility.

showed an irreversible oxidation wave and reversible reduction wave (Figure S7 in the Supporting Information). The peak oxidation potential was −0.09 V versus Fc/Fc^+, and QA-OH had a sufficient electron-donating ability to cause air oxidation. The half-wave reduction potential was −1.69 V, which was negatively shifted from that of QA-BF_2 (−1.00 V).

Figure 5 shows the energy diagram of the HOMOs and LUMOs of QA-BF_2 and its related compounds obtained *via* DFT calculations at the B3LYP/6-31G(d) level. Because QA-BF_2 is a reduced form of QQ-BF_2, the HOMO and LUMO energies of QA-BF_2 are higher than those of QQ-BF_2, respectively. The LUMO energy of QA-BF_2 is higher than that of DHND-BF_2 (−3.76 eV), and the LUMO energy of QQ-BF_2 is much lower that of DHND-BF_2. Furthermore, the HOMO and LUMO energies increase in the order of QA-BF_2, monoBF_2, and QA-OH, and the HOMO-LUMO

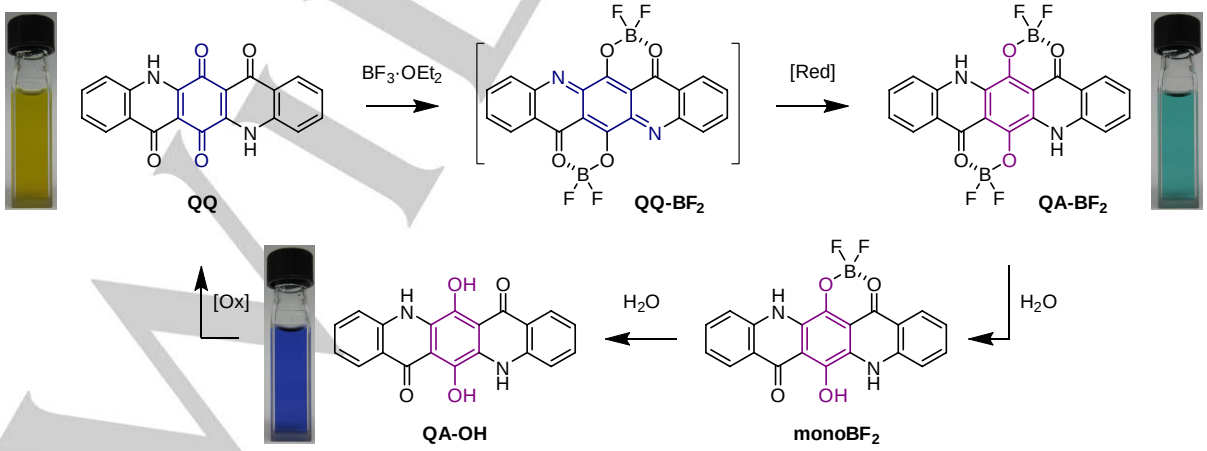

Scheme 2. Formation of QA-BF_2 from QQ and regeneration of QQ *via* monoBF_2 and QA-OH.

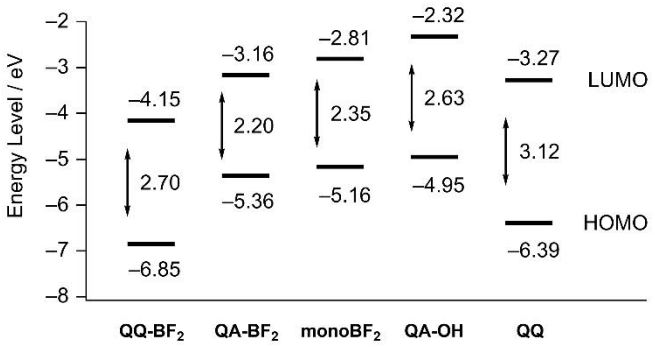

Figure 5. HOMO and LUMO energies [eV] of QA-BF_2 and its related compounds calculated *via* DFT at the B3LYP/6-31G(d) level.

energy. This indicates that the electronic properties depend on the number of boron chelates. The space arrangements of HOMO and LUMO are similar among these compounds and are delocalized on the whole quinacridone moiety (Figure S8 in the Supporting Information). This theoretical energy diagram supported the nature of the BF_2 complexes observed in the UV/Vis spectra and CV experiments.

QA-OH was obtained as a dark purple solid from a solution of QA-BF_2 in DMSO containing 5 vol% of water at 90 °C in argon (Supporting Information). We also succeeded in obtaining a dark blue single crystal (M.p. 293–294 °C) suitable for X-ray crystallography.[23] Since it was a good crystal with $R_1 = 0.049$ [$I > 2\sigma(I)$], all hydrogen atoms were determined from the difference Fourier map and were refined. The molecular structure is centrosymmetric and planar (Figure 6A), and the bond lengths in the central six-membered ring are almost the same to those as QA-BF_2 (Figure 6B). The C–O single bond is 1.351(2) Å, and the C–C distances are 1.395(3), 1.408(3), and 1.413(3) Å. In the 4(1*H*)-pyridone moieties, the C–O double bond is 1.256(2) Å. The crystal contains two DMSO molecules per QA-OH molecule, and QA-OH is surrounded by six DMSO molecules (Figure 6C). The DMSO molecules are in contact with OH, CO, and NH moieties of QA-OH *via* hydrogen bonds. Therefore, QA-OH was found to be stable in air in the solid state despite easy air oxidation in solution. The QA-OH molecules stacked with an average interplanar distance of 3.29 Å, forming a herringbone structure along the *b* axis (Figure 6D). The herringbone angle is 82°. This packing structure is characterized by a stacking pair and edge-to-edge pairs, as shown in Table S1 (Supporting Information). The value of electronic coupling for hole transfer was calculated to be 48 and 5 meV for the stacking and edge-to-edge pairs, respectively. The reorientation energy was determined to be 319 meV. From these values, a hole mobility of 0.05 $cm^2\ V^{-1}\ s^{-1}$ was theoretically obtained. This value was slightly lower than the experimental and theoretical values of QA (0.2 $cm^2\ V^{-1}\ s^{-1}$).[20a]

In conclusion, we studied BF_2 chelation to quinacridonequinone (QQ). Since the generated BF_2 complex (QQ-BF_2) possesses a strong electron affinity, its reduced form (QA-BF_2) is produced as a dark green solid. This compound is stable in the solid state, whereas it underwent hydrolysis in solution to produce 6,13-dihydroxyquinacridone (QA-OH) in

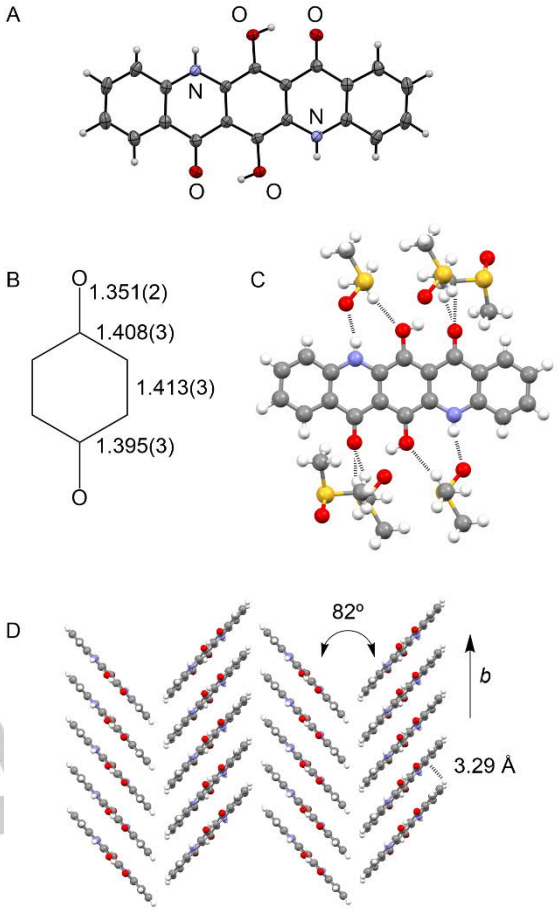

Figure 6. Crystal structure of QA-OH: A) molecular structure drawn at the 50% probability level (ORTEP), B) bond lengths [Å] in the central six-membered ring, C) hydrogen bonds with DMSO molecules, and D) the herringbone structure.

argon. Although QA-OH is air sensitive owing to its strong electron-donating ability, we succeeded in obtaining it as a dark purple solid. Therefore, the BF_2 chelation of QQ is a new and convenient synthetic method for deriving from QQ to QA-OH. Moreover, QQ was regenerated by air oxidation of QA-OH in solution. QA-OH also behaved as a reducing reagent, *e.g.*, converting benzoquinone to hydroquinone. Since QA-OH can be easily generated upon the hydrolysis of a QA-BF_2 solution, it may be used as an organic reducing reagent and oxygen sensor. These compounds are also applicable to organoelectronics as functional pigments because they have characteristic absorptions of green or blue color.

Acknowledgements

This work was supported by JSPS KAKENHI Grant Number JP15K05422. We thank Prof. Dr. Hidehiro Uekusa (Tokyo Institute of Technology) and Dr. Masaaki Tomura (Institute for Molecular Science) for their advice on the X-ray crystallographic studies. We also thank Prof. Dr. Motonori Watanabe (Kyushu University) for his advice on the mobility calculations. The DFT

calculations were performed at the Research Center for Computational Science (Okazaki) and the Center for Computational Materials Science of the Institute for Materials Research (Tohoku University).

Conflict of interest

The authors declare no conflict of interest.

Keywords: Boron • Chelates • Dyes/Pigments • Hydrolysis • Reduction

[1] a) P.-Z. Chen, L.-Y. Niu, Y.-Z. Chen, Q.-Z. Yang, *Coord. Chem. Rev.* **2017**, *350*, 196–216; b) K. Tanaka, Y. Chujo, *NPG Asia Mater.* **2015**, *7*, e223.

[2] a) R. Yoshii, A. Nagai, K. Tanaka, Y. Chujo, *Chem. Eur. J.* **2013**, *19*, 4506–4512; b) R. Yoshii, A. Hirose, K. Tanaka, Y. Chujo, *Chem. Eur. J.* **2014**, *20*, 8320–8324; c) P.-Z. Chen, Y.-X. Weng, L.-Y. Niu, Y.-Z. Chen, L.-Z. Wu, C.-H. Tung, Q.-Z. Yang, *Angew. Chem.* **2016**, *128*, 2809–2813; *Angew. Chem. Int. Ed.* **2016**, *55*, 2759–2763; d) F. Ito, Y. Suzuki, J. Fujimori, T. Sagawa, M. Hara, T. Seki, R. Yasukuni, M. L. de la Chapelle, *Sci. Rep.* **2016**, *6*, 22918; e) P. Galer, R. C. Korošec, M. Vidmar, B. Šket, *J. Am. Chem. Soc.* **2014**, *136*, 7383–7394.

[3] a) A. Sakai, E. Ohta, Y. Matsui, S. Tsuzuki, H. Ikeda, *ChemPhysChem* **2016**, *17*, 4033–4036; b) Z. Yu, Y. Wu, L. Xiao, J. Chen, Q. Liao, J. Yao, H. Fu, *J. Am. Chem. Soc.* **2017**, *139*, 6376–6381; c) M. Koch, K. Perumal, O. Blacque, J. A. Garg, R. Saiganesh, S. Kabilan, K. K. Balasubramanian, K. Venkatesan, *Angew. Chem.* **2014**, *126*, 6496–6500; *Angew. Chem. Int. Ed.* **2014**, *53*, 6378–6382.

[4] a) P.-H. Lanoë, B. Mettra, Y. Y. Liao, N. Calin, A. D'Aléo, T. Namikawa, K. Kamada, F. Fages, C. Monnereau, C. Andraud, *ChemPhysChem* **2016**, *17*, 2128–2136; b) E. Cogné-Laage, J.-F. Allemand, O. Ruel, J.-B. Baudin, V. Croquette, M. Blanchard-Desce, L. Jullien, *Chem. Eur. J.* **2004**, *10*, 1445–1455.

[5] a) K. Ono, H. Yamaguchi, K. Taga, K. Saito, J. Nishida, Y. Yamashita, *Org. Lett.* **2009**, *11*, 149–152; b) K. Ono, J. Hashizume, H. Yamaguchi, M. Tomura, J. Nishida, Y. Yamashita, *Org. Lett.* **2009**, *11*, 4326–4329; c) Y. Kubota, T. Niwa, J. Jin, K. Funabiki, M. Matsui, *Org. Lett.* **2015**, *17*, 3174–3177.

[6] J. Fabian, H. Hartmann, *J. Phys. Org. Chem.* **2004**, *17*, 359–369.

[7] a) R. Yoshii, K. Suenaga, K. Tanaka, Y. Chujo, *Chem. Eur. J.* **2015**, *21*, 7231–7237; b) G. Zhang, J. Lu, M. Sabat, C. L. Fraser, *J. Am. Chem. Soc.* **2010**, *132*, 2160–2162; c) G. R. Krishna, R. Devarapalli, R. Prusty, T. Liu, C. L. Fraser, U. Ramamurty, C. M. Reddy, *IUCrJ* **2015,** *2*, 611–619; d) M. Louis, A. Brosseau, R. Guillot, F. Ito, C. Allain, R. Métivier, *J. Phys. Chem. C* **2017**, *121*, 15897–15907.

[8] a) K. Kamada, T. Namikawa, S. Senatore, C. Matthews, P.-F. Lenne, O. Maury, C. Andraud, M. Ponce-Vargas, B. Le Guennic, D. Jacquemin, P. Agbo, D. D. An, S. S. Gauny, X. Liu, R. J. Abergel, F. Fages, A. D'Aléo, *Chem. Eur. J.* **2016**, *22*, 5219–5232; b) X. Zhang, Y. Tian, Z. Li, X. Tian, H. Sun, H. Liu, A. Moore, C. Ran, *J. Am. Chem. Soc.* **2013**, *135*, 16397–16409; c) G. Zhang, G. M. Palmer, M. W. Dewhirst, C. L. Fraser, *Nat. Mater.* **2009**, *8*, 747–751.

[9] a) H. Maeda, K. Naritani, Y. Honsho, S. Seki, *J. Am. Chem. Soc.* **2011**, *133*, 8896–8899; b) A. Kuno, N. Tohnai, N. Yasuda, H. Maeda, *Chem. Eur. J.* **2017**, *23*, 11357–11365.

[10] a) D.-H. Kim, A. D'Aléo, X.-K. Chen, A. D. S. Sandanayaka, D. Yao, L. Zhao, T. Komino, E. Zaborova, G. Canard, Y. Tsuchiya, E. Choi, J. W. Wu, F. Fages, J.-L. Brédas, J.-C. Ribierre, C. Adachi, *Nat. Photonics* **2018**, *12*, 98–104; b) A. D'Aléo, M. H. Sazzad, D. H. Kim, E. Y. Choi, J. W. Wu, G. Canard, F. Fages, J.-C. Ribierre, C. Adachi, *Chem. Commun.* **2017**, *53*, 7003–7006.

[11] Y. Mizuno, Y. Yisilamu, T. Yamaguchi, M. Tomura, T. Funaki, H. Sugihara, K. Ono, *Chem. Eur. J.* **2014**, *20*, 13286–13295.

[12] C.-T. Poon, D. Wu, V. W.-W. Yam, *Angew. Chem.* **2016**, *128*, 3711–3715; *Angew. Chem. Int. Ed.* **2016**, *55*, 3647–3651.

[13] a) K. Ono, A. Nakashima, Y. Tsuji, T. Kinoshita, M. Tomura, J. Nishida, Y. Yamashita, *Chem. Eur. J.* **2010**, *16*, 13539–13546; b) Y. Sun, D. Rohde, Y. Liu, L. Wan, Y. Wang, W. Wu, C. Di, G. Yu, D. Zhu, *J. Mater. Chem.* **2006**, *16*, 4499–4503.

[14] a) C. A. DeRosa, M. Kolpaczynska, C. Kerr, M. L. Daly, W. A. Morris, C. L. Fraser, *ChemPlusChem* **2017**, *82*, 399–406; b) C. A. DeRosa, S. A. Seaman, A. S. Mathew, C. M. Gorick, Z. Fan, J. N. Demas, S. M. Peirce, C. L. Fraser, *ACS Sens.* **2016**, *1*, 1366–1373.

[15] a) M. Tsuchikawa, A. Takao, T. Funaki, H. Sugihara, K. Ono, *RSC Adv.* **2017**, *7*, 36612–36616; b) G. R. Kumar, P. Thilagar, *Dalton Trans.* **2014**, *43*, 3871–3879; c) Y. Koyama, T. Matsumura, T. Yui, O. Ishitani, T. Takata, *Org. Lett.* **2013**, *15*, 4686–4689.

[16] a) L. Wang, K. Wang, B. Zou, K. Ye, H. Zhang, Y. Wang, *Adv. Mater.* **2015**, *27*, 2918–2922; b) R. Yoshii, A. Hirose, K. Tanaka, Y. Chujo, *J. Am. Chem. Soc.* **2014**, *136*, 18131–18139; c) A. Hirose, K. Tanaka, R. Yoshii, Y. Chujo, *Polym. Chem.* **2015**, *6*, 5590-5595; d) C.-T. Poon, W. H. Lam, V. W.-W. Yam, *Chem. Eur. J.* **2013**, *19*, 3467–3476.

[17] a) G. Hirata, H. Maeda, *Org. Lett.* **2018**, *20*, 2853–2856; b) B. Štefane, *Org. Lett.* **2010**, *12*, 2900–2903; c) B. Štefane, S. Polanc, *Tetrahedron* **2009**, *65*, 2339–2343; d) B. Štefane, S. Polanc, *New J. Chem.* **2002**, *26*, 28–32.

[18] E. F. Paulus, F. J. J. Leusen, M. U. Schmidt, *CrystEngComm* **2007**, *9*, 131–143; b) S. S. Labana, L. L. Labana, *Chem. Rev.* **1967**, *67*, 1–18.

[19] a) C. Wang, D. Chen, W. Chen, S. Chen, K. Ye, H. Zhang, J. Zhang, Y. Wang, *J. Mater. Chem. C* **2013**, *1*, 5548–5556; b) J. Liu, B. Gao, Y. Cheng, Z. Xie, Y. Geng, L. Wang, X. Jing, F. Wang, *Macromolecules* **2008**, *41*, 1162–1167.

[20] a) E. D. Głowacki, M. Irimia-Vladu, M. Kaltenbrunner, J. Gąsiorowski, M. S. White, U. Monkowius, G. Romanazzi, G. P. Suranna, P. Mastrorilli, T. Sekitani, S. Bauer, T. Someya, L. Torsi, N. S. Sariciftci, *Adv. Mater.* **2013**, *25*, 1563–1569; b) E. D. Głowacki, L. Leonat, M. Irimia-Vladu, R. Schwödiauer, M. Ullah, H. Sitter, S. Bauer, N. S. Sariciftci, *Appl. Phys. Lett.* **2012**, *101*, 023305; c) I. Osaka, M. Akita, T. Koganezawa, K. Takimiya, *Chem. Mater.* **2012**, *24*, 1235–1243.

[21] a) H.-J. Song, D.-H. Kim, E.-J. Lee, S.-W. Heo, J.-Y. Lee, D.-K. Moon, *Macromolecules* **2012**, *45*, 7815–7822; b) J. J.-A. Chen, T. L. Chen, B. Kim, D. A. Poulsen, J. L. Mynar, J. M. J. Fréchet, B. Ma, *ACS Appl. Mater. Interfaces* **2010**, *2*, 2679–2686.

[22] A synthesis of QA-OH was reported in 1962, and it was prepared by treating QQ with copper powder in 70% sulfuric acid.[18b] However, despite industrial interests, little studies on QA-OH and its derivatives have been reported.

[23] CCDC 1886674 (QA-BF_2) and 1886675 (QA-OH) contain the supplementary crystallographic data for this paper. These data can be obtained free of charge from The Cambridge Crystallographic Data Centre.

[24] X-ray crystallographic data of CCDC 196985 and 131965 are used for the structures of QA and AQ, respectively.

[25] Gaussian 16 (Revision B.01). Wallingford, CT: Gaussian, Inc., **2016**.

Entry for the Table of Contents (Please choose one layout)

Redox Chemistry

COMMUNICATION

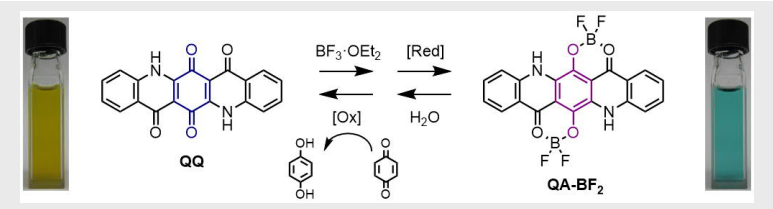

BF_2 chelation to quinacridonequinone (QQ) was performed. The resulting dark green solid was a BF_2 complex of 6,13-dihydroxyquinacridone (QA-OH) and was determined to be QA-BF_2. This compound underwent hydrolysis in argon to produce QA-OH as a dark purple solid. Furthermore, QA-OH was converted to QQ by air oxidation or in the presence of benzoquinone. In this study, a new synthetic method from QQ to QA-OH *via* BF_2 complexes was found.

*K. Moriya, R. Shimada, K. Ono**

Page No. – Page No.

Difluoroboron Chelation to Quinacridonequinone: A New Synthetic Method for Air-Sensitive 6,13-Dihydroxyquinacridone *via* Boron Complexes